NANO LETTERS

2007
Vol. 7, No. 11
3477−3482

Amine–Gold Linked Single-Molecule Circuits: Experiment and Theory

Su Ying Quek,[†] Latha Venkataraman,[‡,§] Hyoung Joon Choi,[||] Steven G. Louie,[†,⊥] Mark S. Hybertsen,[§,#] and J. B. Neaton*[,†]

Molecular Foundry, Lawrence Berkeley National Laboratory, Berkeley, California 94720, Department of Applied Physics, Columbia University, New York, New York 10027, Center for Electron Transport in Nanostructures, Columbia University, New York, New York 10027, Department of Physics and IPAP, Yonsei University, Seoul 120-749, Korea, Department of Physics, University of California, Berkeley, Berkeley, California 94720, and Center for Functional Nanomaterials, Brookhaven National Laboratory, Upton, New York 11973

Received August 15, 2007; Revised Manuscript Received September 6, 2007

ABSTRACT

A combination of theory and experiment is used to quantitatively understand the conductance of single-molecule benzenediamine–gold junctions. A newly developed analysis is applied to a measured junction conductance distribution, based on 59 000 individual conductance traces, which has a clear peak at 0.0064 G_0 and a width of ±47%. This analysis establishes that the distribution width originates predominantly from variations in conductance across different junctions rather than variations in conductance during junction elongation. Conductance calculations based on density functional theory (DFT) for 15 distinct junction geometries show a similar spread. We show explicitly that differences in local structure have a limited influence on conductance because the amine–Au bonding motif is well-defined and flexible, explaining the narrow distributions seen in the experiments. The minimal impact of junction structure on conductance permits an unambiguous comparison of calculated and measured conductance values and a direct assessment of the widely used DFT theoretical framework. The average calculated conductance (0.046 G_0) is found to be seven times larger than experiment. This discrepancy is explained quantitatively in terms of electron correlation effects to the molecular level alignments in the junction.

Discovering the anatomy of single-molecule electronic circuits, in order to exploit their transport behavior, poses fundamental challenges to nanoscience.[1] Single-molecule manipulation requires probes at the limits of experimental resolution,[2−7] as control at the single-bond scale is necessary for reliable transport properties. The success of amine−Au links for the realization of single-molecule electrical junctions has allowed systematic measurements of the relationship between molecular-scale structure and conductance for several families of molecules.[6,8,9] Experimental trends were explained based on the hypothesis of selective bonding between the amine lone pair and an undercoordinated gold atom.[8] Understanding the essential junction features that lead to reproducible electrical properties would enable generalization to other metal−molecule link chemistries while also furthering the development of a predictive theoretical approach to nanoscale transport.

Most recent theoretical investigations of nanoscale transport rely on a Landauer approach, simplified to treat electronic interactions at a mean-field level within density functional theory (DFT). While this framework has proven relatively accurate for metallic point contacts,[10] and certain molecular junctions such as H_2,[11,12] in the majority of cases, the computed conductance often substantially exceeds measured values in junctions with organic molecules,[2,13−17] raising questions about fundamental theoretical approximations. However, since the predicted conductance can be extremely sensitive to contact geometry, changing by orders of magnitude for thiol−Au junctions,[14,15,18] for instance, uncertainty over junction structure has obscured an unambiguous, quantitative comparison between theory and experiment for single-molecule conductance. A clear benchmark is required.

In this Letter, we use the reproducible conductance of amine−gold linked single-molecule circuits[6,8,9] to develop a detailed, atomic-scale understanding of a prototypical molecular junction. An in-depth analysis of a large experimental data set for benzenediamine (BDA) is provided and directly compared with DFT-based transport calculations to clarify the origin of the spread in the conductance distribu-

* Corresponding author. E-mail: jbneaton@lbl.gov.
[†] Molecular Foundry, Lawrence Berkeley National Laboratory.
[‡] Department of Applied Physics, Columbia University.
[§] Center for Electron Transport in Nanostructures, Columbia University.
[||] Department of Physics and IPAP, Yonsei University.
[⊥] Department of Physics, University of California, Berkeley.
[#] Center for Functional Nanomaterials, Brookhaven National Laboratory.

10.1021/nl072058i CCC: $37.00 © 2007 American Chemical Society
Published on Web 09/27/2007

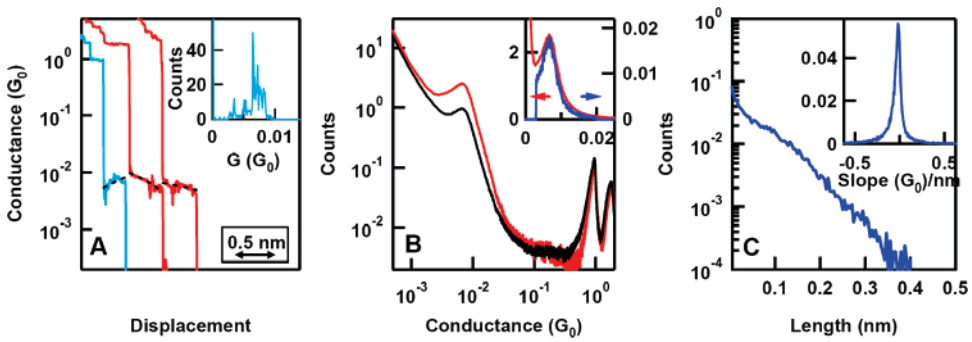

Figure 1. (a) Sample conductance vs displacement traces measured while displacing the sample relative to the tip at 16 nm/s. Dashed black lines are linear fits to the molecular step determined by an automated algorithm (applied bias is 25 mV). Inset: Histogram of the blue conductance trace computed by binning the conductance data (acquired at 40 kHz) using a 10^{-4} G_0 bin size. (b) Conductance histograms of all 59 000 measured traces (black) and of 21 312 selected traces with steps (red), both computed with a bin size of 10^{-4} G_0 shown on a log−log scale, and normalized to the number of traces. Inset: Normalized conductance histogram of traces with molecular steps (red, left axis) and normalized histogram of step-average conductance (blue, right axis) computed with a bin size of 10^{-4} G_0 shown on a linear scale. (c) Normalized histograms of step lengths (main panel; bin size is 0.004 G_0/nm, shown on a semilog scale) and step slopes (inset; bin size is 0.0025 G_0/nm, shown on a linear scale) determined from automated fitting algorithm.

tion. Our calculations explicitly show that the amine−gold bonding is highly selective, but flexible, explaining the relative insensitivity of the conductance to junction structure. Although the computed conductance has a narrow spread consistent with experiment, the average calculated conductance is ∼7× larger. Since the junction structure does not significantly affect conductance, our comparison provides a benchmark that directly demonstrates the importance of many-electron corrections beyond DFT.

To obtain a detailed picture of junction structure that can be connected to its transport properties, we use a newly developed analysis of a series of conductance traces obtained at low-bias from BDA−Au junctions formed by repeatedly breaking Au point contacts in a molecular solution.[8] Many conductance traces reveal a step below 1 G_0 ($2e^2/h$) (Figure 1a), corresponding to a single BDA molecule between the two atomic point contacts.[6,8] Figure 1b shows the histogram (black) computed from all 59 000 measured traces, from four different tip/sample pairs, without any data selection. The most probable junction conductance obtained from Lorentzian[6] fits to the histogram peak is 0.0064 ± 0.0005 G_0, with half width 47 ± 8%. These values are in good agreement with previous reports.[6]

We now extend our previous analysis to establish whether the measured spread is dominated by variations in conductance (i) within each measured trace (i.e., due to changes in the junction structure during elongation) or (ii) across measured traces. First, we note that not all measured conductance traces have a step at a value near the molecular peak in the full histogram (black, Figure 1b). An automated sorting algorithm is developed and used to determine if a trace has a step between 0.003 and 0.02 G_0 (Figure 1a, see Supporting Information). For each trace with a step, its average conductance is calculated with a linear fit, the "step-average conductance". Our analysis indicates that about 36% of the traces have a molecular step. The distributions of step lengths and step slopes determined from the linear fits are shown in Figure 1c. We find that the majority of steps (∼75%) are <1 Å long, with a power law distribution extending to about 4 Å. Further, ∼75% of the steps are flat, with a slope around −0.1 G_0/nm. Further insight is gained from comparing the distribution of step-average conductances (see Supporting Information) in traces with a molecular step (blue histogram in Figure 1b inset) to that obtained by binning all data points in the traces that have molecular steps (red histogram in Figure 1b inset). The conductance peak position and half width are 0.0065 (0.0065) G_0 and ±40 (45)% for the blue (red) histograms, in excellent agreement with those for the full histogram from all traces (black). The spread in the step-average histogram (blue) accounts for most of the overall spread in the red histogram. Together with the fact that most steps are short and flat, we can conclude that the spread in the measured conductance originates primarily from variations in conductance *across* different junctions rather than variations in conductance during junction elongation just before breaking.

The repeated plastic deformation of the contact region from measurement to measurement induces variations in atomic structure across junctions. Understanding the impact of junction structure on conductance is critical. We approach this problem in two steps. Using first-principles DFT, possible bonding motifs in the junction are analyzed to probe the selective bonding hypothesis.[8] Then, guided by allowed bonding motifs, 15 distinct junction structures are examined to relate the conductance to junction structure. Further details of our calculations can be found in the Supporting Information.

Unlike thiol−Au linkages,[15] we find that the local amine−Au bonding motif is remarkably well-defined, with the amine group only binding to undercoordinated Au atop sites. If the amine group is initially positioned at the bridge or threefold site between Au atoms, the molecule is found to relax to the nearest atop site or drift away from the Au contact. Furthermore, typical BDA binding energies on undercoordinated Au sites (0.4 to 0.6 eV) are significantly larger than that on the atop site of atomically flat Au(111) (0.1 eV), in accord with previous DFT calculations on alkanediamines.[8] This provides detailed support for the initial hypothesis:[8] the strongly basic amine group readily donates its lone pair to form Au−N bonds with an undercoordinated Au atom where

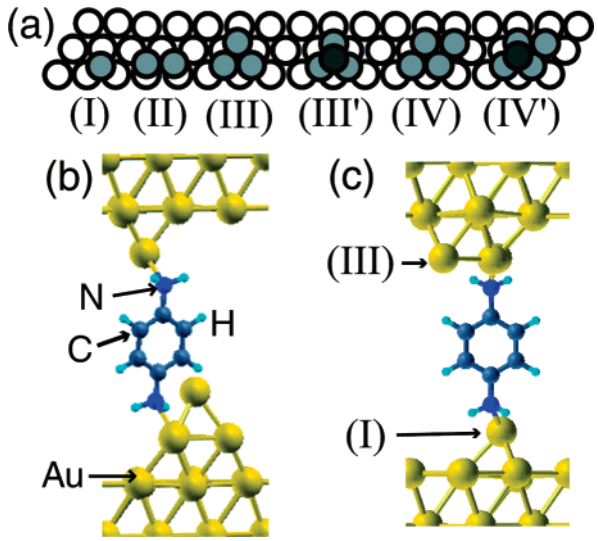

Figure 2. (a) Au contact motifs, (b) "side" junction, (c) (III, I) junction. In (b), one amine group is bonded to an adatom (I), and the other to an atom at the base of a pyramid (III′). The molecule is bonded in a *trans* configuration in (b) and (c), where the Au atom at opposite contacts are on opposite sides of the molecular plane. The molecular tilt angle (angle between the Au surface normal and the N−N axis) is 10° in (b) and 0° in (c). All junctions have translational symmetry parallel to the surface plane, with each supercell containing 16 Au atoms per layer.

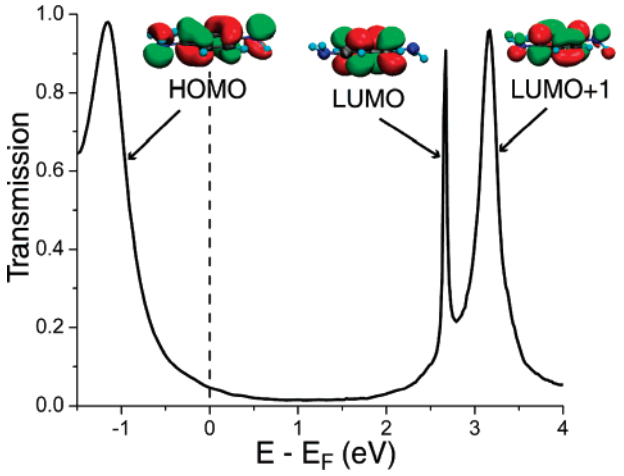

Figure 3. Energy-dependent transmission for the (III, I) junction. Isosurface plots illustrate the molecular orbitals responsible for the transmission peaks.

the 6*s* orbital is more available, in contrast to the relatively unreactive sites on flat Au(111).[8]

Drawing on the specific character of the amine−Au bonding motif, we next develop model contact geometries with variations in junction structure, considering a total of 15 fully relaxed molecular junctions. These geometries differ in the molecular tilt angle (0°, 10°, 31°, and 56° with Au surface normal), bonding configuration (*cis*/*trans*), binding sites, and Au contact structures. Both symmetric and asymmetric junctions are examined. Six distinct Au contact structures with varying degrees of coordination are considered (Figure 2a). Except for the "side" junction in Figure 2b, all other junctions are labeled according to its two Au contact structures (e.g., (III, I) in Figure 2c). The calculated binding energy for the BDA bonded to two gold contacts varies modestly among the 15 junction structures (0.8−1.3 eV) (Supplementary Table 1).

The conductance is computed from the Landauer formula, evaluated using electronic states from a self-consistent potential obtained with DFT in an energy- and $k_{||}$-dependent scattering state approach[16] (Supporting Information). Figure 3 shows a typical calculated transmission curve, $T(E)$, at zero bias, obtained for the (III, I) junction. The peaks centered at −1.2, 2.7, and 3.2 eV derive respectively from the BDA highest occupied molecular orbital (HOMO), lowest unoccupied molecular orbital (LUMO), and LUMO + 1 states. The transmission for all 15 junctions is plotted on a log scale in Figure 4a and illustrates the remarkably narrow spread in $T(E)$ near E_F. Moreover, for all junctions, the transmission from ∼−1.5 to 0.5 eV is found to be associated with a single eigenchannel[19] arising from the BDA HOMO, consistent with experiment.[9] For the 15 junctions considered here, the calculated linear response conductance $G_0\,T(E_F)$ has a mean value of 0.046 G_0 and ranges from 0.032 (−31.1%) to 0.062 (+35.4%) G_0. This spread, which is similar to the half-width observed in the histogram of measured step-average conductances (inset, Figure 1b), provides the first quantitative explanation for the narrow measured conductance distribution: junction conductances are relatively insensitive to detailed atomic configurations that can vary across measured traces. The calculated conductance magnitude, however, exceeds the measured value by about a factor of 7.

The geometric feature with the greatest impact on $T(E)$ is n, the total number of Au nearest neighbors of the two Au binding sites. The right (high-energy) tail of the resonance peak, centered at ∼−1 eV, is well fit to a Lorentzian form $T(E) = A/((E - E_0)^2 + (\Gamma/2)^2)$, for each junction with $n > 6$ (Figure 4b). For those junctions with $n = 6$, additional structure in $T(E)$ appears near E_F. The relatively good fits for $n > 6$ reflect a modest electronic coupling between the BDA HOMO and an approximately constant density of states (DOS). The structure in $T(E)$ near E_F for $n = 6$ is due to additional features in the projected DOS on the Au contacts (Figure 4b inset), which arise from the interaction of bulk and surface states with the *s*-like orbitals of the undercoordinated adatom. Overall, the transmission resonance energy E_0 (−1.27 to −0.94 eV) and peak width Γ (0.34−0.56 eV) exhibit modest variation (Supplementary Table 1). Further, the small increase in peak width Γ with coordination n leads to an increase in conductance, evident from the comparison of the Lorentzian conductance (predicted from the fit) with the calculated conductance in Figure 4c. However, the extra structure in $T(E)$ for $n = 6$ results in an enhanced conductance beyond the Lorentzian model, a partial compensation reducing the variation of conductance with n.

From the experimental and theoretical results, we can conclude that the local amine−Au bonding motif does not vary significantly across different junction geometries. Large changes in the molecular tilt angle and bonding configuration can be accommodated with relatively small variations in the Au−N−C bond angles (which range from 112° to 130°) and

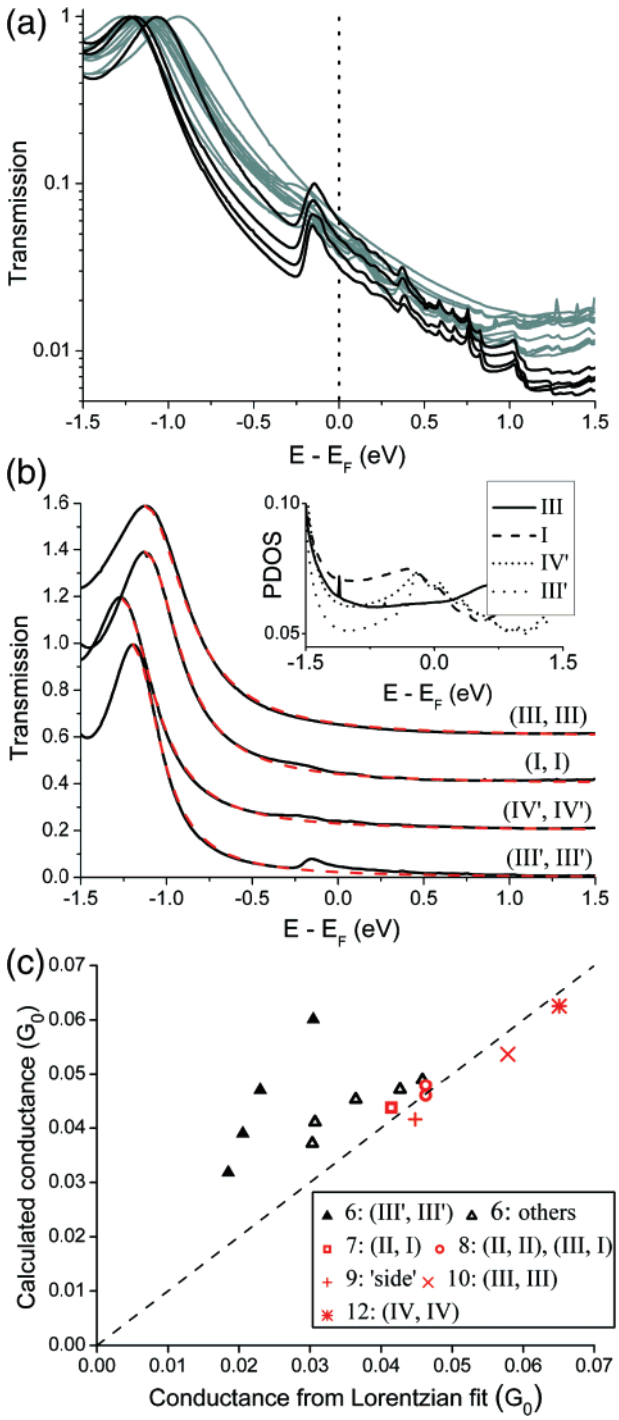

Figure 4. Calculated transmission curves plotted on (a) a log scale for all 15 junction geometries, and (b) a linear scale for four representative geometries, vertically offset for clarity. Inset: Scattering state PDOS on Au binding sites, in the absence of the molecule. (c) Calculated conductance vs conductance predicted from Lorentzian fits (red dashed lines in (b)). Numbers in the legend refer to *n* described in the text. The resonances centered at ~−1 eV have a maximum transmission of 0.97−0.99 G_0. Black curves in (a) correspond to (III′, III′) junctions, which have the most additional structure in transmission near E_F, as indicated in (b).

N−Au bond lengths (which range from 2.38 to 2.55 Å). Due to the intrinsic isotropy of the Au 6*s* orbital, modest variations in local bond lengths and angles have minimal impact on the electronic coupling at the low biases relevant here.

The experimental analysis indicates that the junction-elongation process does not contribute significantly to the spread in conductance (Figure 1). Most of the measured steps in the conductance traces are relatively short, consistent with the junction breaking at the N−Au bond.[20] The longer steps in the tail of the distribution may involve changes in the molecular tilt angle, or shifting of the N lone pair from one Au site to another before final breaking. Upon stretching of the "side" junction (Figure 2b) to simulate breaking (Supporting Information), our calculations indicate that the N lone pair moves from its original binding site at the base of the Au pyramid to the atom at the apex of the pyramid. Since the conductance for these two configurations is similar, this process would appear as a single step. However, with an energy barrier (~0.3 eV) that is similar to the work done on the junction computed to elongate it to maximum force (~0.2 eV for ~0.5 nN), such events should be less common.

Having established that the junction structure has minimal impact on conductance in BDA−Au junctions, we now provide a direct assessment of the widely used DFT framework for computing conductance. Our calculations overestimate the conductance by about a factor of 7. Given the relatively small effects of junction geometry on conductance, this discrepancy is unlikely to arise from finite temperature fluctuations. Instead, the deviation likely originates from the use of mean-field theory based on DFT. Indeed, many-electron interactions are essential to accurately position frontier molecular resonance energies in a junction, and the DFT errors can be large.[21] Direct treatment of such interactions in transport through molecules is challenging and, to date, studies have been confined to model systems.[22−29] However, many-electron interactions are expected to reduce the DFT conductance, shifting the molecular resonances away from E_F[21,25,26] and narrowing the transmission peak widths in the weak coupling limit.[24,26] Working with the Lorentzian form established above for the HOMO resonance transmission, we find that either reducing its width (Γ) from ~0.5 to ~0.2 eV or shifting its position (E_0) from −1 to −3 eV relative to E_F would bring the calculated conductance in line with the measured value.

Given the relative structural insensitivity of its conductance, experimental data from the BDA−Au junction is clearly valuable for future benchmarks of many-electron approaches to conductance. However, further analysis of the present results already provides insight into the nature and magnitude of the errors in standard DFT conductance calculations. On physical grounds, the resonance position E_0 is too shallow because of self-energy errors inherent to the use of (LDA or) GGA Kohn−Sham (KS) eigenvalues as quasiparticle energies.[21,30] The self-energy corrections to the KS eigenvalues for small aromatic molecules are expected to be significant and large, whereas such corrections for metallic bulk and surface Au states would be relatively much smaller, especially for states near E_F. For the gas-phase BDA molecule, a comparison between the experimentally measured[31] ionization potential and the GGA HOMO eigenvalue (relative to vacuum) implies a self-energy correction of $\Sigma_0^{HOMO} \sim -3$ eV (Figure 5a). However, electrostatic polar-

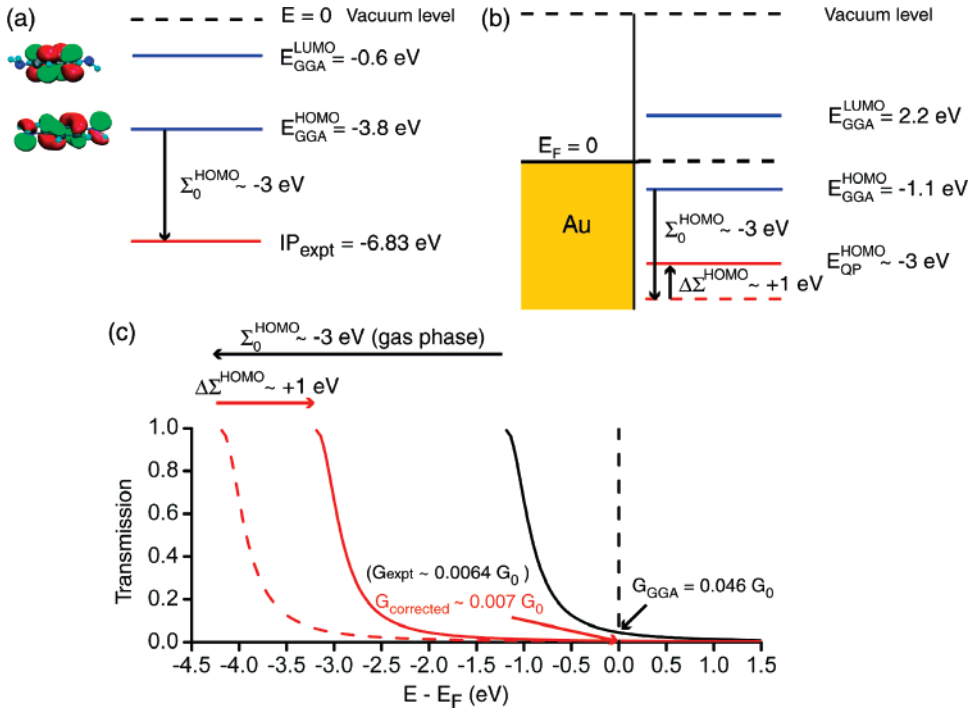

Figure 5. Energy level diagrams showing self-energy corrections in (a) the gas phase and (b) the junction. Σ_0^{HOMO} refers to the self-energy correction to the GGA HOMO eigenvalue, E_{GGA}^{HOMO}, in the gas phase. In the junction, polarization effects result in a further self-energy correction, $\Delta\Sigma^{HOMO}$, to E_{GGA}^{HOMO}. The net self-energy correction to E_{GGA}^{HOMO} in the junction is given by $\Sigma^{HOMO} = \Sigma_0^{HOMO} + \Delta\Sigma^{HOMO}$, which is ~ -2 eV in this case. (c) Changes in transmission curve and conductance due to self-energy correction to the HOMO level in the (II, II) junction. Black: DFT transmission. Solid red: transmission curve after E_{GGA}^{HOMO} has been shifted to the estimated quasiparticle HOMO level, E_{QP}^{HOMO}, in the junction. The self-energy correction to E_{GGA}^{LUMO} is calculated to be $\sim +2$ eV. The LUMO resonance is thus shifted upward, further away from E_F, and will not contribute to the low bias conductance.

ization of the Au contacts and, to a lesser extent, the surrounding solvent, further modifies the electron-removal energy (HOMO level) in the junction[21] by an amount $\Delta\Sigma^{HOMO}$. To estimate $\Delta\Sigma^{HOMO}$, we use a simple, physically motivated image charge model, which has been shown to capture the shift in electron addition and removal energies of aromatic molecules weakly coupled to metallic substrates.[21] In the present case, we calculate within this picture $\Delta\Sigma^{HOMO}$ to be $\sim +1$ eV, using an image plane position of ~ 1 Å (from the Au surface atomic plane) and taking the electron position to be at the center of the benzene ring, ~ 5 Å from the substrate for a typical geometry considered here.[31] This results in a large net self-energy correction for the HOMO resonance position in the junction, $\Sigma^{HOMO} = \Sigma_0^{HOMO} + \Delta\Sigma^{HOMO}$, of ~ -2 eV (Figure 5b). This large net self-energy correction shifts the HOMO level from ~ -1 to ~ -3 eV and results in a conductance in good agreement with experiment, as illustrated in Figure 5c for the (II, II) junction. Similar arguments apply to the net self-energy correction for the LUMO orbital energy, which we compute to be approximately equal and opposite to that for the HOMO. The LUMO resonance is thus shifted away from E_F, upward by $\sim +2$ eV and will not contribute to the low bias conductance. Our self-energy correction to the DFT-GGA HOMO orbital energy, together with the fact that the conductance is relatively insensitive to junction geometry, can explain the discrepancy between the DFT conductance and experiment for this system. Since the low bias conductance is determined by transmission through the slowly varying tail of the HOMO-derived resonance, these shifts significantly alter the conductance, but they minimally affect the other calculated trends.

Acknowledgment. Portions of this work were performed at the Molecular Foundry, Lawrence Berkeley National Laboratory, and were supported by the Office of Science, Office of Basic Energy Sciences, of the U.S. Department of Energy under Contract No. DE-AC02-05CH11231. This work was partially supported by the Nanoscale Science and Engineering Initiative of the NSF (award numbers CHE-0117752 and CHE-0641532), the New York State Office of Science, Technology, and Academic Research (NYSTAR) and by NSF grant no. DMR04-39768. Portions of this work were performed at the Center for Functional Nanomaterials, Brookhaven National Laboratory, and was supported by the Office of Science, Office of Basic Energy Sciences, of the U.S. Department of Energy under contract number DE-AC0298CH10886. Portions of the computational resources required for this work were provided by NERSC.

Supporting Information Available: Experimental procedure, data analysis procedure (Supplementary Figure 1), theoretical method, details of theoretical results (Supplementary Table 1), references. This information is available free of charge via the Internet at http://pubs.acs.org.

References

(1) Nitzan, A.; Ratner, M. A. *Science* **2003**, *300*, 1384−1389.
(2) Reed, M. A.; Zhou, C.; Muller, C. J.; Burgin, T. P.; Tour, J. M. *Science* **1997**, *278*, 252−254.
(3) Reichert, J.; Ochs, R.; Beckmann, D.; Weber, H. B.; Mayor, M.; von Lohneysen, H. *Phys. Rev. Lett.* **2002**, *88*, 176804-1−176804-4.
(4) Liang, W. J.; Shores, M. P.; Bockrath, M.; Long, J. R.; Park, H. *Nature* **2002**, *417*, 725−729.
(5) Xu, B. Q.; Tao, N. J. J. *Science* **2003**, *301*, 1221−1223.
(6) Venkataraman, L.; Klare, J. E.; Nuckolls, C.; Hybertsen, M. S.; Steigerwald, M. L. *Nature* **2006**, *442*, 904−907.
(7) Moresco, F.; Meyer, G.; Rieder, K. H.; Tang, H.; Gourdon, A.; Joachim, C. *Phys. Rev. Lett.* **2001**, *86*, 672−675.
(8) Venkataraman, L.; Klare, J. E.; Tam, I. W.; Nuckolls, C.; Hybertsen, M. S.; Steigerwald, M. L. *Nano Lett.* **2006**, *6*, 458−462.
(9) Venkataraman, L.; Park, Y. S.; Whalley, A. C.; Nuckolls, C.; Hybertsen, M. S.; Steigerwald, M. L. *Nano Lett.* **2007**, *7*, 502−506.
(10) Nielsen, S. K.; Brandbyge, M.; Hansen, K.; Stokbro, K.; van Ruitenbeek, J. M.; Besenbacher, F. *Phys. Rev. Lett.* **2002**, *89*, 066804-1−066804-4.
(11) Smit, R. H. M.; Noat, Y.; Untiedt, C.; Lang, N. D.; van Hemert, M. C.; van Ruitenbeek, J. M. *Nature* **2002**, *419*, 906−909.
(12) Thygesen, K. S.; Jacobsen, K. W. *Phys. Rev. Lett.* **2005**, *94*, 036807-1−036807-4.
(13) Basch, H.; Cohen, R.; Ratner, M. A. *Nano Lett.* **2005**, *5*, 1668−1675.
(14) Stokbro, K.; Taylor, J.; Brandbyge, M.; Mozos, J. L.; Ordejon, P. *Comput. Mater. Sci.* **2003**, *27*, 151−160.
(15) Tomfohr, J.; Sankey, O. F. *J. Chem. Phys.* **2004**, *120*, 1542−1554.
(16) Choi, H. J.; Cohen, M. L.; Louie, S. G. *Phys. Rev. B* **2007**, submitted for publication.
(17) Dadosh, T.; Gordin, Y.; Krahne, R.; Khivrich, I.; Mahalu, D.; Frydman, V.; Sperling, J.; Yacoby, A.; Bar-Joseph, I. *Nature* **2005**, *436*, 677−680.
(18) Muller, K. H. *Phys. Rev. B* **2006**, *73*, 045403-1−045403-6.
(19) Brandbyge, M.; Sorensen, M. R.; Jacobsen, K. W. *Phys. Rev. B* **1997**, *56*, 14956−14959.
(20) Li, Z.; Kosov, D. S. 2007, arXiv:cond-mat/0702507.
(21) Neaton, J. B.; Hybertsen, M. S.; Louie, S. G. *Phys. Rev. Lett.* **2006**, *97*, 216405.
(22) Toher, C.; Filippetti, A.; Sanvito, S.; Burke, K. *Phys. Rev. Lett.* **2005**, *95*, 146402−1-146402−4.
(23) Delaney, P.; Greer, J. C. *Phys. Rev. Lett.* **2004**, *93*, 036805-1−036805-4.
(24) Ferretti, A.; Calzolari, A.; Di Felice, R.; Manghi, F.; Caldas, M. J.; Nardelli, M. B.; Molinari, E. *Phys. Rev. Lett.* **2005**, *94*, 116802-1−116802-4.
(25) Darancet, P.; Ferretti, A.; Mayou, D.; Olevano, V. *Phys. Rev. B* **2007**, *75*, 075102-1−075102-4.
(26) Koentopp, M.; Burke, K.; Evers, F. *Phys. Rev. B* **2006**, *73*, 121403-1−121403-4.
(27) Sai, N.; Zwolak, M.; Vignale, G.; Di Ventra, M. *Phys. Rev. Lett.* **2005**, *94*, 186810-1−186810-4.
(28) Thygesen, K. S.; Rubio, A. *J. Chem. Phys.* **2007**, *126*, 091101.
(29) Ke, S. H.; Baranger, H. U.; Yang, W. T. *J. Chem. Phys.* **2007**, *126*, 4.
(30) Hybertsen, M. S.; Louie, S. G. *Phys. Rev. B* **1986**, *34*, 5390−5413.
(31) Linstrom, P. J.; Mallard, W. G. *NIST Chemistry WebBook*; NIST Standard Reference Database Number 69; National Institute of Standards and Technology: Gaithersburg MD, 2005; http://webbook.nist.gov, 20899.

NL072058I